Available online at www.sciencedirect.com
ScienceDirect
Trans. Nonferrous Met. Soc. China 25(2015) 2594−2600
Transactions of Nonferrous Metals Society of China
www.tnmsc.cn

Corrosion properties of stainless steel 316L/Ni−Cu−P coatings in warm acidic solution

Xin-xian FANG[1,2], Heng-zhi ZHOU[1,2], Ya-jun XUE[1,2]

1. Jiangsu Key Laboratory of Advanced Structural Materials and Application Technology, Nanjing 211167, China;
2. School of Materials Engineering, Nanjing Institute of Technology, Nanjing 211167, China

Received 13 October 2014; accepted 10 March 2015

Abstract: In order to improve corrosion resistance of stainless steel 316L in warm acidic solution, Ni−Cu−P coatings with high copper and phosphorus contents were deposited onto stainless steel 316L substrates via electroless plating. The structure of the film and its resistance to corrosion in a warm acidic environment were investigated using scanning electron microscopy (SEM), energy dispersive spectroscopy (EDS), X-ray diffraction spectrometry (XRD), polarization curves, electrochemical impedance spectroscopy (EIS), and dipping corrosion tests, respectively. The results demonstrate that Ni−Cu−P coatings consist of two types of nodules, which are 19.98% Cu and 39.17% Cu (mass fraction) respectively. The corrosion resistance of the 316L substrate when subjected to a warm acidic solution is significantly improved by the addition of the new type of the Ni−Cu−P coating. The as-plated coatings demonstrate better corrosion resistance than annealed coatings. As-plated coatings and those annealed at 673 K are found to corrode selectively, while pitting is observed to be the main corrosion mechanism of coatings annealed at 773 and 873 K.
Key words: Ni−Cu−P coating; stainless steel 316L; corrosion resistance; corrosion mechanism; warm acidic solution

1 Introduction

Ni−Cu−P coatings have extensive potential applications in industry, as they offer many characteristics, such as thermal stability [1,2], corrosion resistance [3,4], solderability [5,6], and magnetic and electrical properties [7], which are superior to those of electroless Ni−P coatings. LIU et al [8] reported that an electroless 84.7%Ni−8.6%Cu−6.23%P coating offered better corrosion resistance in flue gas condensate than an as-plated Ni−P coating or the Cu substrate. LIU and ZHAO [9] further found that the anti-corrosion performance of a Ni−Cu−P coating in 1.0 mol/L HCl solution was improved by using a copper content of 17.2%. ZHAO et al [10] demonstrated that both the deposition rate and the coating composition may be varied by increasing the content of $CuSO_4·5H_2O$ in the deposition bath. Moreover, they found that a Ni−Cu−P−PTFE coating with 6.5% Cu displayed the highest corrosion resistance of all the studied coatings when tested in 1 mol/L HCl solution, and that the performance of this coating also surpassed that of a Ni−P−PTFE coating and the bare Cu sheet. Our previous study [3] indicated that the corrosion rate suffered by an electroless 79.63%Ni−7.04%Cu−13.33%P coating in 3.68 mol/L H_2SO_4 solution was lower than that of a simple Ni−P coating and unmodified 316L stainless steel. It has been reported that Ni−Cu−P coatings have excellent corrosion resistance in acidic media [8,9] and the corrosion tests discussed above were carried out at room temperature. As such, the corrosion behavior of these coatings in warm acidic solutions has yet to be described.

Stainless steel is a commonly used material for the fabrication of metal components which are to be exposed to acidic media. PARDO et al [11] demonstrated that the corrosion rate of 316L in 30% H_2SO_4 (mass fraction) was increased by about one order of magnitude with the increase of medium temperature from 25 to 50 °C. In addition, the corrosion process of 316L was inhibited at 25 °C and revealed general corrosion attack at 50 °C. This means that stainless steel is extremely susceptible to corrosion in warm acidic solutions since the corrosion product layer of 316L cannot provide a significant corrosion protection, thereby limiting its use in certain

Foundation item: Project (CKJA201202) supported by the Innovation Fund Key Project of Nanjing Institute of Technology, China; Project (51301088) supported by the National Natural Science Foundation of China
Corresponding author: Xin-xian FANG; Tel: +86-25-86118287; E-mail: fangxinxian@njit.edu.cn
DOI: 10.1016/S1003-6326(15)63880-8

applications. It was reported that the Ni−P coatings containing more than 10% P are more resistant to attack than those with lower phosphorus content in acidic environment [12], and the Ni−Cu−P coatings with higher Cu content exhibit higher corrosion resistance [13]. Thus, in the present work, a coating of 68.25%Ni−21.54%Cu−10.21%P was deposited on the surface of 316L samples using an electroless plating technique. The corrosion behavior of the coatings in 3.68 mol/L H_2SO_4 solution at 323 K, as well as that of unmodified 316L substrates, was investigated. The effect of annealing temperature on the corrosion resistance of the Ni−Cu−P coatings was also studied.

2 Experimental

Cold-rolled stainless steel 316L sheets (9.64% Ni, 16.33% Cr, 1.16% Mn, 2.54% Mo, 70.33% Fe, mass fraction) with dimensions of 15 mm × 15 mm × 1 mm were used as substrates for the preparation of electroless Ni−Cu−P coatings. Prior to electroless deposition, 316L sheets were cleaned at 358 K for 30 min in an alkaline solution containing 40 g/L NaOH, 30 g/L Na_2CO_3, and 15 g/L Na_3PO_4. Substrates were then pickled for 1−3 min in an activation solution consisting of 150 mL/L H_2SO_4 (98% H_2SO_4) and 20 g/L NaCl. Subsequently, Ni−Cu−P coatings were electrolessly deposited on the 316L substrates.

The Ni−Cu−P electroless plating bath was composed of 20 g/L nickel sulfate, 6 g/L copper sulfate, 22 g/L sodium hypophosphate, 40 g/L sodium citrate, and 20 g/L sodium acetate. The bath temperature was maintained at (355±1) K using an HHS−1 water bath pan and the pH of the bath was controlled to be 10.0−10.5 using NaOH. The plating time was 2 h. After the electroless plating process, an isothermal heat treatment was performed to anneal samples. The samples were annealed at 573, 673, 723, 773, 823 and 873 K for 2 h.

The corrosion rate, v_0, was tested with immersion corrosion tests. Samples of as-plated and annealed Ni−Cu−P coating substrates were immersed in 3.68 mol/L H_2SO_4 solution at 323 K for 5 h. The mass of the samples was measured with an FA1004-type electronic balance (accuracy of 0.1 mg). The corrosion rate was calculated as $v_0=\Delta m_1/(St)$, where Δm_1 is the mass loss experienced by the sample, S is the surface area of sample, and t is the test length.

A PARSTAT2273 electrochemical workstation was used to carry out potentiodynamic polarization and electrochemical impedance spectroscopy measurements. The measurements were performed using a conventional three-electrode cell, in which a sample of as-plated or annealed Ni−Cu−P coating stainless steel was placed in an epoxide resin holder. Using this holder, the surface area of the sample that was exposed to the corrosive medium was approximately 1 cm^2. A 1 cm×1 cm square platinum strip was served as the counter electrode and a saturated calomel electrode (SCE) was used as the reference electrode. EIS measurements at an open circuit potential were carried out over a frequency range of 0.1 Hz to 100 kHz with an AC amplitude of 5 mV. After EIS measurements were made, potentiodynamic polarization measurements were performed over a voltage range of ±250 mV around the corrosion potential with a scan rate of 4 mV/s. All measurements were conducted in 3.68 mol/L H_2SO_4 solution at 323 K.

The morphology and composition of the coating surfaces were analyzed using a JSM6360LVX scanning electron microscope and a GENESIS2000XMS60 energy dispersive spectroscope, respectively. The structures of the as-plated and annealed deposits were studied using a conventional continuous scanning X-ray diffraction method with an Ultma IV diffractometer. Based on the XRD results, the sizes of the nanometer-scale Ni(Cu), Ni_3P and Cu_3P grains were calculated according to the following Scherrer formula:

$$D=K\lambda/(\beta_m\cos\ \theta) \quad (1)$$

where D is the mean size of the nanometer grain; λ is the X-ray wavelength (λ=1.5418 Å); θ is the angle of the diffraction peak, β_m is the half-peak width for the appropriate diffraction peak in rad, and K is the Scherrer constant.

3 Results and discussion

3.1 Effect of heat treatment on microstructure

The surface morphology of the as-plated Ni−Cu−P coating consists of white nodules distributed evenly on a surface of interconnected grey spherical nodules (Fig. 1). A higher-magnification observation of a white nodule reveals that the top surface of the structure shows even finer nodular and flower-like growth. EDS analysis was carried out on an overview of the sample, as well as the grey and white regions. As shown in Table 1, the results demonstrate that the Ni−Cu−P coating is composed of two types of nodules with different compositions, with the grey nodules having lower Cu and higher P contents than the white nodules. The white nodule may be attributed to the special growth process of electroless deposition. In this system, both Cu^{2+} and Ni^{2+} can be reduced by NaH_2PO_2 to produce Cu and Ni. The contents of Ni and Cu reduced by NaH_2PO_2 in different positions of the substrate are different since the reduction potentials of Ni and Cu are quite different [14], which leads to the formation of white nodule structure in Cu-rich position and that of grey nodule structure in poor Cu position.

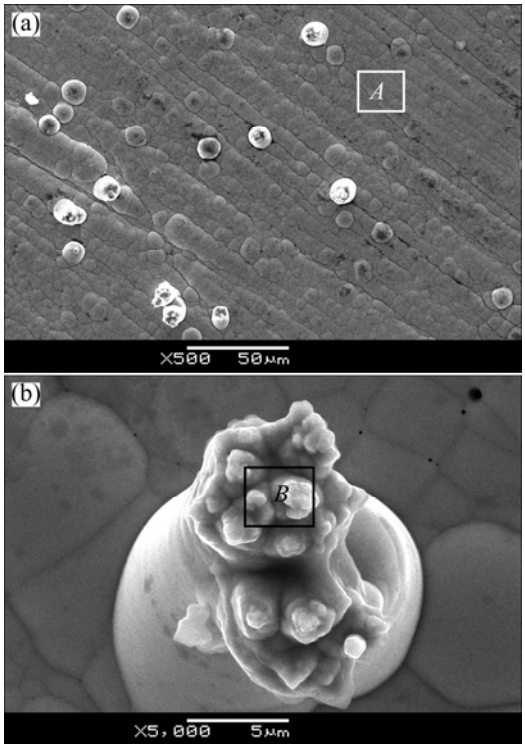

Fig. 1 Surface morphologies of Ni−Cu−P coating (a) and white spherical nodule (b)

Table 1 Elemental compositions of as-plated Ni−Cu−P coatings in Fig. 1

Region	Mass fraction/%		
	Ni	Cu	P
Grey region (*A*)	68.98	19.98	11.04
White region (*B*)	52.11	39.17	8.72
Overall region	68.25	21.54	10.21

The surface morphologies of the annealed Ni−Cu−P coatings were also observed by SEM, which are similar to those of as-plated Ni−Cu−P coating (Fig. 2(a)). The XRD spectra of the studied coatings can be found in Fig. 2(b). A weak, broad peak situated at 2θ=42°−45° was detected for both the as-plated coatings and those annealed at 573 K, indicating that the Ni−Cu−P coating is still amorphous when it is annealed at low temperatures. However, upon increasing the annealing temperature to over 673 K, sharp diffraction peaks which are characteristic of the crystalline phases of Ni(Cu), Ni_3P and Cu_3P can be observed. The gradual increase in the intensities of these peaks demonstrates that the Ni−Cu−P coating gradually transforms from amorphous to crystalline. In addition, diffraction peaks which can be ascribed to NiO and CuO phases are also observed, which suggests the existence of an oxide film on the surface of the coatings.

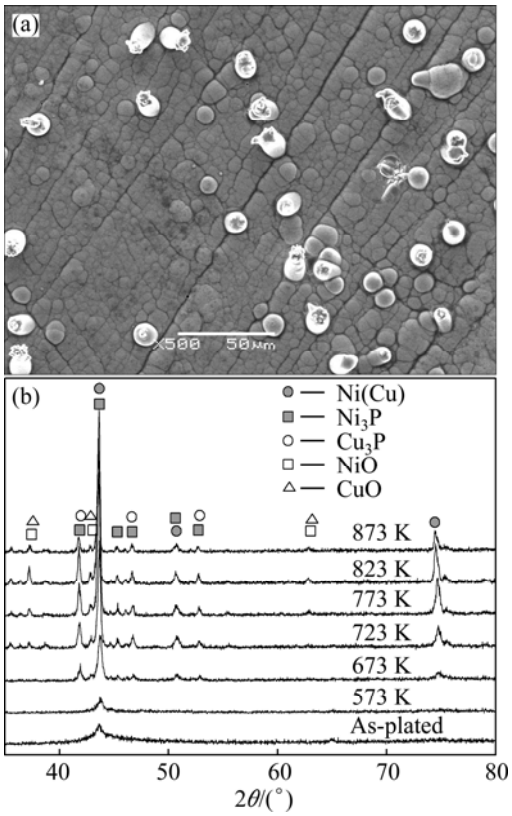

Fig. 2 Surface morphology of Ni−Cu−P coating annealed at 400 °C (a) and XRD patterns of Ni−Cu−P coatings (b)

Figure 3 shows the variation of the grain sizes of Ni(Cu), Ni_3P and Cu_3P with annealing temperature. The grain sizes are all on the nanoscale although they increase with increasing the annealing temperature, resulting in nanocrystalline Ni−Cu−P coatings after annealing.

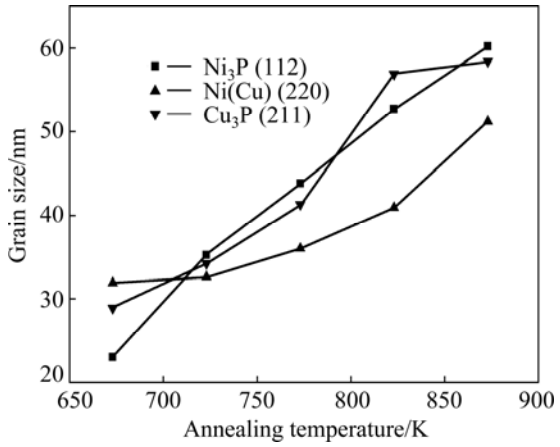

Fig. 3 Variation of grain size of Ni(Cu), Ni_3P and Cu_3P with annealing temperature

3.2 Effect of heat treatment on corrosion rate and corrosion mechanism

The corrosion rates of the bare 316L stainless steel

and the samples coated with Ni−Cu−P are compared in Fig. 4. It is clear that the deposition of a Ni−Cu−P coating onto a 316L substrate can greatly reduce the corrosion rate suffered by a sample. Amorphous Ni−Cu−P coatings show better corrosion resistance than nanocrystalline coatings because these samples are free from grain boundaries, dislocations, and so forth. Among the nanocrystalline Ni−Cu−P coatings produced after annealing at 673 K (sample NC4), 773 K (NC5) and 873 K (NC6), sample NC5 demonstrates the best anti-corrosion performance.

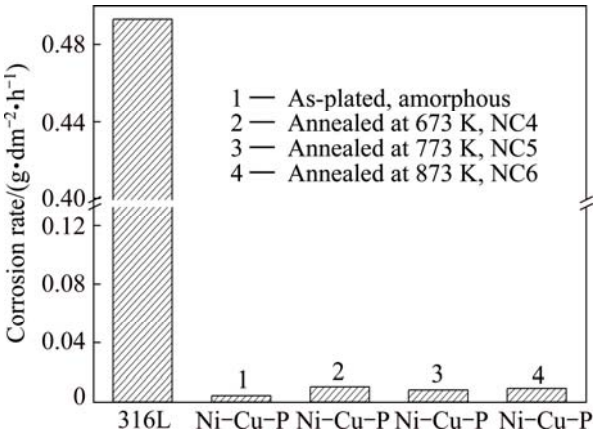

Fig. 4 Corrosion rates of 316L with or without Ni−Cu−P coating in 3.68 mol/L H_2SO_4 solution at 323 K

After the immersion corrosion tests, the surface morphologies of coatings were again examined with SEM (Fig. 5). The morphology of the corroded surface of the amorphous coating is similar to that of the fresh surface (Fig. 1(a)). A compositional analysis with EDS shows that the Ni, Cu and P contents of this sample are 66.25%, 23.54% and 10.22%, respectively. The Ni content of the corroded sample is slightly lower than that of the original coating (Table 1), indicating that preferential dissolution of Ni occurs during corrosion and that the corrosion occurs by a slightly selective mechanism.

The morphology of the corroded surface of sample NC4 displays a few white flower-like structures distributed on a surface of flat grey nodule (Fig. 5(b)). The results of a compositional analysis of an overview of this sample, including both the grey and the white regions, are collected in Table 2. Combined with the results shown in Fig. 1 and Table 1, it can be concluded that the white flower-like structures are the residues of corrosion of the copper-rich nodular structures, wherein drastically preferential dissolution of Ni and P results in very low Ni and P contents in the post-corrosion structure. The Cu content of the grey region of Sample NC4 also slightly decreases after corrosion, suggesting a similar corrosion mechanism to that seen for the amorphous coating.

Figures 5(c) and (d) show the corroded surface morphologies of Samples NC5 and NC6, respectively. The surface morphologies of these samples differ significantly from those of the amorphous coating and Sample NC4. Visible etching pits are evenly distributed on the corroded surfaces of Samples NC5 and NC6, indicating that both samples underwent pitting corrosion. EDS analysis shows that the mass fractions of Ni, Cu, P and O are 77.01%, 10.13%, 4.91% and 7.95% for

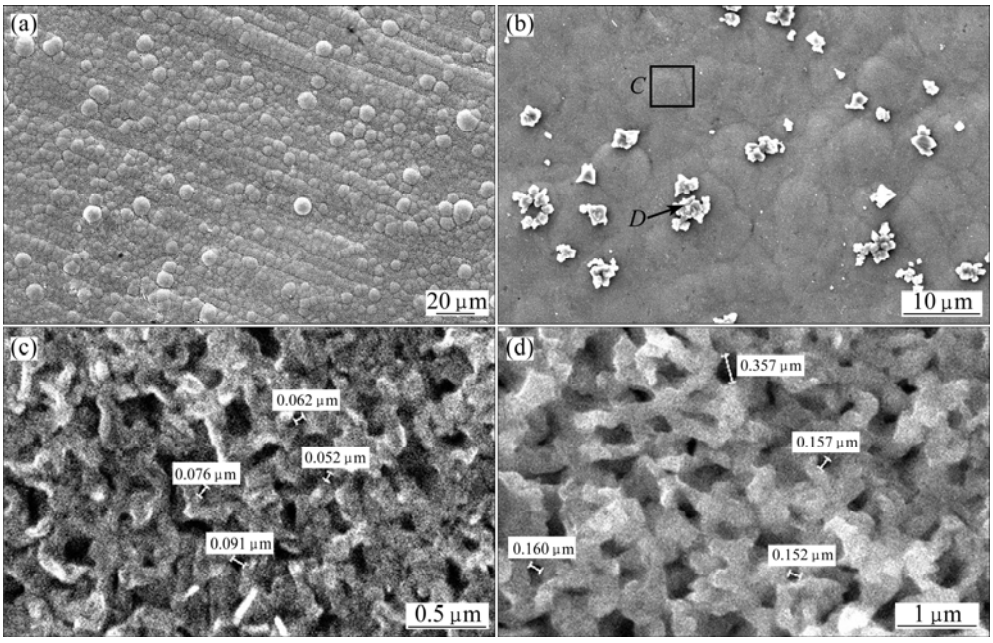

Fig. 5 SEM images of corroded surface of Ni−Cu−P coatings in 3.68 mol/L H_2SO_4 solution at 323 K for 5 h: (a) Amorphous; (b) NC4; (c) NC5; (d) NC6

Table 2 Corroded surface compositions of Sample NC4 in Fig. 5(b)

Region	Mass fraction/%		
	Ni	Cu	P
Grey region (*C*)	71.58	17.50	10.92
White region (*D*)	9.50	89.27	1.23
Overall region	68.30	21.40	10.30

Sample NC5, and 85.25%, 5.16%, 1.58% and 8.01% for Sample NC6. The Cu and P contents of these samples are also drastically decreased compared with the composition of the original Ni−Cu−P coating (Table 1). In addition, by referring the pre-corrosion grain sizes found in Fig. 3, it can be observed that the sizes of the etching pits on the corroded surfaces of Samples NC5 and NC6 are close to the grain size of $Ni_3P(Cu_3P)$. This implies that the pits are formed by the dissolution or peeling of Cu_3P grains. Moreover, the size of the holes is larger than that of $Ni_3P(Cu_3P)$ particles due to deep corrosion of inter surface of holes after the solution of $Ni_3P(Cu_3P)$.

3.3 Polarization measurements

The polarization curves of 316L with or without a Ni−Cu−P coating are shown in Fig. 6, while the corrosion potentials (φ_{corr}) and corrosion current densities (J_{corr}) can be found in Table 3. Compared with the bare 316L substrate, the coated 316L exhibits higher corrosion potential and lower corrosion current density. Among the Ni−Cu−P coatings, corrosion current density of the amorphous coating is lower than those of the nanocrystalline coatings. Sample NC5 shows the lowest corrosion current density among the studied nanocrystalline coatings. These results are in good agreement with the results of the immersion corrosion test.

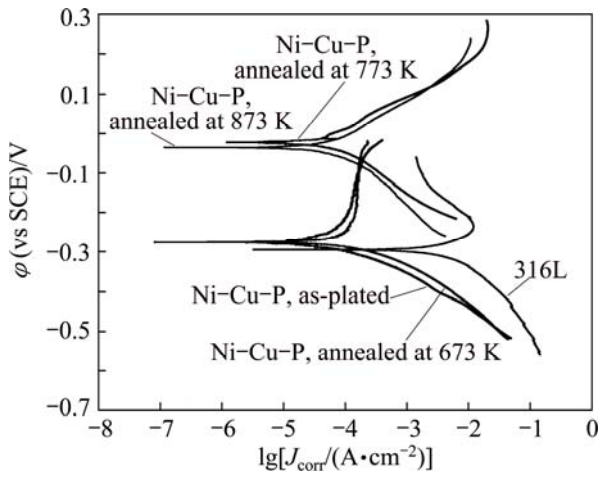

Fig. 6 Potentiodynamic polarization curves of 316L with or without Ni−Cu−P coatings

Table 3 Values of φ_{corr} and J_{corr} of 316L with or without Ni−Cu−P coatings

Material	φ_{corr}(vs SCE)/mV	J_{corr}/(A·cm^{-2})
316L substrate	−296.0	4.93×10^{-3}
Ni−Cu−P coating, amorphous	−275.8	7.80×10^{-5}
Ni−Cu−P coating, NC4	−275.8	1.30×10^{-4}
Ni−Cu−P coating, NC5	−22.4	8.10×10^{-5}
Ni−Cu−P coating, NC6	−36.5	1.00×10^{-4}

3.4 Electrochemical impedance spectroscopy

Figure 7 shows the Nyquist and Bode plots of coated and uncoated 316L. The Nyquist plot of the bare 316L consists of two capacitive arcs and one inductive arc, whereas the Nyquist plot of the sample with amorphous coating and that of Sample NC5 show a single capacitive arc. A low frequency tail beside the capacitive arc can be seen in the plots of Samples NC4 and NC6.

For the bare 316L, the first capacitive arc at high frequencies corresponds to the combined effect of double-layer capacitance and metal dissolution and its diameter is related to the charge transfer resistance at the metal−solution interface. Since general corrosion attack in 30% H_2SO_4 (mass fraction) at 50 °C occurred for the bare 316L [11], the second capacitive arc at middle frequencies may be explained through the generation of a second path of dissolution of adsorbed corrosion product [15], and the inductive behavior observed at low frequencies for 316L may be attributed to the formation of corrosion product [16]. In comparison with the samples of 316L with Ni−Cu−P coatings, the values of capacitance arc radius, impedance ($|Z|$), and phase angle (θ) are smaller for the bare 316L. This suggests that the resistance to corrosion of 316L can be unambiguously improved by the addition of an electroless plated Ni−Cu−P coating.

In comparing the results of the samples prepared with Ni−Cu−P coatings, it can be seen that the as-plated coating exhibits higher values of capacitance arc radius, impedance ($|Z|$), and maximum phase angle (θ_{max}) than the annealed coatings. So, it can be concluded that the annealing process has an adverse effect on the anticorrosion properties of Ni−Cu−P coatings in a warm acidic environment.

Impedance data were fitted using ZSimpWin3.10 software. The resulting equivalent circuits, shown in Fig. 8, represent the electrochemical behavior at the surface-solution interface of the bare 316L and the Ni−Cu−P coating, respectively. For the bare 316L substrate, a QR_{ct} parallel combination, a $CR1_p$ combination in series, and an LRl_{p1} combination in series are used to fit the high, middle, and low frequency data.

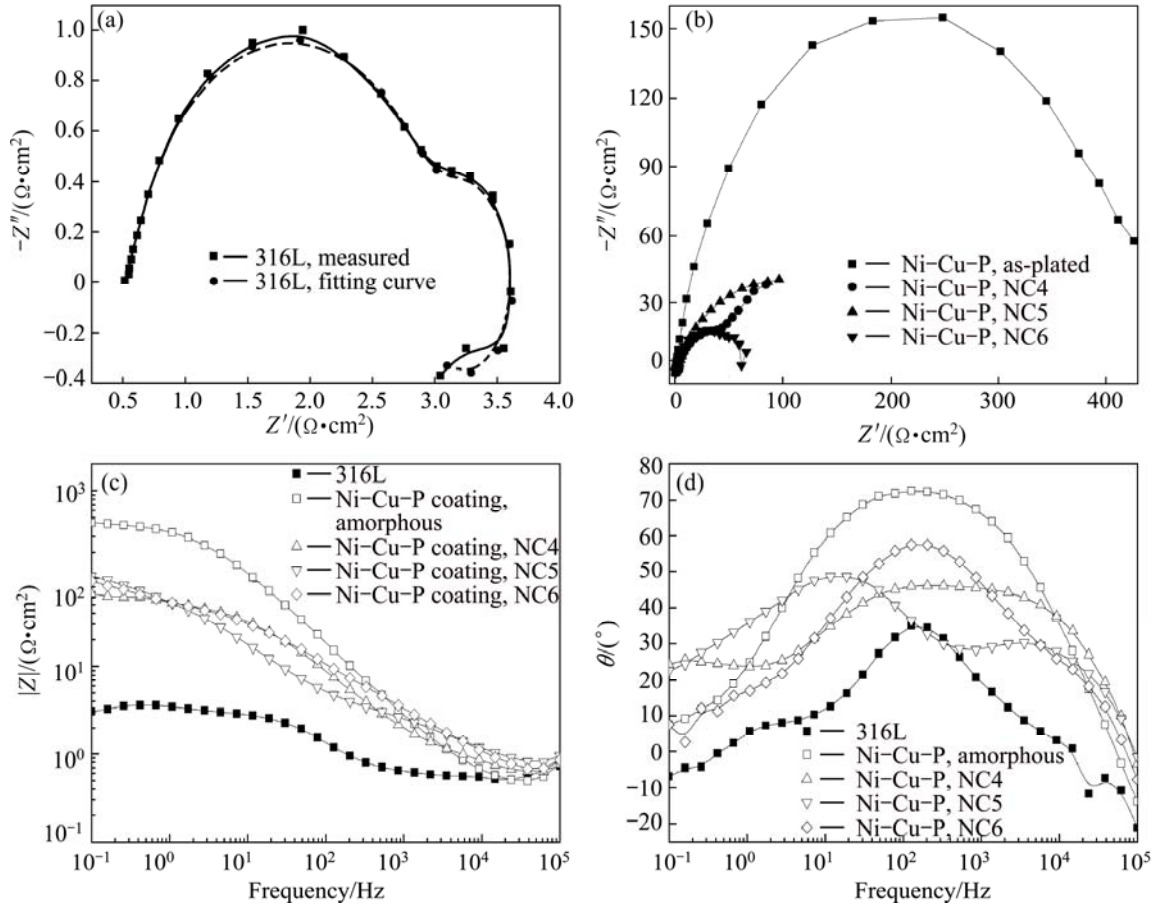

Fig. 7 Nyquist (a,b) and Bode (c,d) plots of 316L with or without Ni−Cu−P coatings

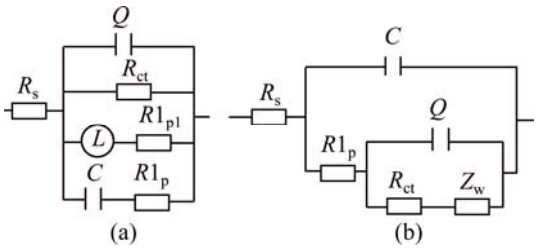

Fig. 8 Equivalent circuits of 316L (a) and Ni−Cu−P coatings (b)

These elements are combined in parallel and placed in series with R_s. R_s represents the solution resistance, Q and R_{ct} are the double-layer capacitance and high-frequency charge transfer resistance, respectively, C and L describe the capacitance and inductance of the corrosion product film, respectively, while Rl_{p1} and Rl_p are the resistances of the corrosion product film at low and middle frequencies, respectively. The equivalent circuit used to describe the behavior of the Ni−Cu−P-coated 316L consists primarily of six elements representing the solution resistance (R_s), coating capacitance (C), coating resistance (Rl_p), double-layer capacitance (Q), charge transfer resistance (R_{ct}), and Warburg impedance (Z_w). As shown in Fig. 7, the experimental impedance data (solid curve) can be fitted very well with the proposed equivalent circuits (dotted curve). The theoretical impedance parameters of the equivalent model suggest that the value of R_{ct} for the bare 316L substrate is lower than that of the Ni−Cu−P coating. Moreover, the existence of inductance at low frequencies indicates that even the formation of a corrosion product film fails to protect the 316L substrate from corrosion in a warm acidic solution. The as-plated coating has the highest value of R_{ct} and therefore the best resistance to corrosion among various Ni−Cu−P coatings, which further reinforces the conclusion that annealing at temperatures between 673 and 873 K has an adverse effect on the corrosion protection performance of the coatings.

4 Conclusions

1) Ni−Cu−P coatings with two types of nodules were deposited on the surface of 316L stainless steel substrates via electroless plating. The coatings provide good protection from corrosion in a warm acidic solution.

2) Heat treatment has a harmful effect on the corrosion resistance of the Ni−Cu−P coatings. Among

the annealed Ni−Cu−P coatings, the coating annealed at 723 K exhibits higher capacitance arc radius, impedance, and lower corrosion current density, corrosion rate than those annealed at 623 K and 823 K.

3) The mechanism of corrosion undergone by the coatings when placed in a warm acidic environment depends on their structures, with selective corrosion occurring in the coatings as-plated and annealed at 623 K, while the coatings annealed at 723 K and 823 K experienced pitting corrosion.

References

[1] HU Y, YANG L, SHI C D, TANG W M. Microstructural evolution and phase transformation kinetics of pulse-electroplated Ni−Cu−P alloy film during annealing [J]. Materials Chemistry and Physics, 2013, 141: 944−950.

[2] ASHASSI-SORKHABI H, DOLATI H, PARVINI-AHMADI N, MANZOORI J. Electroless deposition of Ni−Cu−P alloy and study of the influences of some parameters on the properties of deposits [J]. Applied Surface Science, 2002, 185: 155−160.

[3] FANG Xin-xian, BAI Yun-qiang, WANG Zhang-zhong. Erosion corrosion behavior of J4 stainless steel and electroless plating coatings of Ni−P and Ni−Cu−P in liquid−solid two-phase flow [J]. Acta Metallurgica Sinica, 2010, 46: 239−244. (in Chinese)

[4] ABDEL HAMEED R M, FEKRY A M. Electrochemical impedance studies of modified Ni−P and Ni−Cu−P deposits in alkaline medium [J]. Electrochimica Acta, 2010, 55: 5922−5929.

[5] ZHU L, LUO L M, LUO J, WU Y C, LI J. Effect of electroless plating Ni−Cu−P layer on brazability of cemented carbide to steel [J]. Surface and Coatings Technology, 2012, 206: 2521−2524.

[6] ZHU L, LUO L M, LUO J, LI J, WU Y C. Effect of electroless plating Ni−Cu−P layer on the wettability between cemented carbides and soldering tins [J]. International Journal of Refractory Metals and Hard Materials, 2012, 31: 192−195.

[7] YANG S Q, LIU H P, HAN S M, LI Y, SHEN W Z. Effects of electroless composite plating Ni−Cu−P on the electrochemical properties of La−Mg−Ni-based hydrogen storage alloy [J]. Applied Surface Science, 2013, 271: 210−215.

[8] LIU G C, YANG L J, WANG L D, WANG S L, LIU C Y, WANG J. Corrosion behavior of electroless deposited Ni−Cu−P coating in flue gas condensate [J]. Surface and Coatings Technology, 2010, 204: 3382−3386.

[9] LIU Y, ZHAO Q. Study of electroless Ni−Cu−P coatings and their anti-corrosion properties [J]. Applied Surface Science, 2004, 228: 57−62.

[10] ZHAO Q, LIU Y, ABEL E W. Effect of Cu content in electroless Ni−Cu−P−PTFE composite coatings on their anti-corrosion properties [J]. Materials Chemistry and Physics, 2004, 87: 332−335.

[11] PARDO A, MERINO M C, COY A E, VIEJO F, ARRABAL R, MATYKINA E. Effect of Mo and Mn additions on the corrosion behaviour of AISI 304 and 316 stainless steels in H_2SO_4 [J]. Corrosion Science, 2008, 50: 780−794.

[12] HARI KRISHNAN K, JOHN S, SRINIVASAN K N, PRAVEEN J, GANESAN M, KAVIMANI P M. An overall aspect of electroless Ni−P depositions [J]. Metallurgical and Materials Transactions A, 2006, 37: 1917−1926.

[13] XU Yang, ZOU Yong, LUAN Tao. The effect of Cu content on the properties and electrochemical behavior of electroless Ni−Cu−P coatings [J]. Journal of Functional Materials, 2013, 44: 244−248. (in Chinese)

[14] YU Q Y, ZENG Z X, ZHAO W J, LI M H, WU X D, XUE Q J. Fabrication of adhesive superhydrophobic Ni−Cu−P alloy coatings with high mechanical strength by one step electrodeposition [J]. Colloids and Surfaces A: Physicochemical and Engineering Aspects, 2013, 427: 1−6.

[15] ITAGAKI M, SUZUKI T, WATANABE K. Channel flow double electrode study on anodic dissolution of molybdenum in sulfuric acid solution [J]. Electrochim Acta, 1997, 42: 1081−1086.

[16] KEDDAM M, MATTOS O R, TAKENOUTI H. Mechanism of anodic dissolution of iron-chromium alloys investigated by electrode impedances. I: Experimental results and reaction model [J]. Electrochim Acta, 1986, 31: 1147−1158.

高温酸性溶液中 316L 不锈钢/Ni−Cu−P 镀层的耐蚀性能

方信贤[1,2]，周衡志[1,2]，薛亚军[1,2]

1. 江苏省先进结构材料及应用技术重点实验室，南京 211167；
2. 南京工程学院 材料工程学院，南京 211167

摘 要：为了改善 316L 不锈钢在高温酸性溶液中的耐蚀性，采用化学镀技术在 316L 不锈钢表面沉积高铜高磷 Ni−Cu−P 镀层。采用扫描电镜(SEM)、能谱仪(EDS)和 X 射线衍射仪(XRD)对其结构进行分析，利用极化曲线、阻抗谱(EIS)及浸泡腐蚀试验对其在高温酸性溶液中的耐蚀性进行研究。结果表明，Ni−Cu−P 镀层由铜含量分别为 19.98%和 39.17% (质量分数)两种类型的胞状组织组成；在高温酸性溶液中，这种新型 Ni−Cu−P 镀层可显著改善 316L 不锈钢的耐蚀性；镀态镀层的耐蚀性优于热处理态的；镀态镀层和经 673 K 热处理镀层的腐蚀机制是选择性腐蚀，而经 773 和 873 K 热处理镀层的腐蚀机制为点腐蚀。

关键词：Ni−Cu−P 镀层；316L 不锈钢；耐蚀性；腐蚀机制；高温酸性溶液

(Edited by Wei-ping CHEN)